Interaction between dye and zinc in the dye-dispersing ZnO films prepared by a wet process

Hiromasa Nishikiori,*[1] Takumi Takikawa,[1] Kazuki Ito,[1] Satoshi Nagaya,[2] Hajime Wagata,[1] Katsuya Teshima,[1] Tsuneo Fujii[3]

[1] Department of Environmental Science and Technology, Faculty of Engineering, Shinshu University, 4-17-1, Wakasato, Nagano 380-8553, Japan

[2] Nagano Prefecture General Industrial Technology Center, 1-3-1, Osachi-Katamacho, Okaya, Nagano 394-0084, Japan

[3] Nagano Prefectural Institute of Technology, 813-8 Shimonogo, Ueda, Nagano 386-1211, Japan

Corresponding author: Hiromasa Nishikiori

Phone: +81-26-269-5536

Fax: +81-26-269-5531

E-mail: nishiki@shinshu-u.ac.jp

Department of Environmental Science and Technology, Faculty of Engineering, Shinshu University, 4-17-1, Wakasato, Nagano 380-8553, Japan

Abstract

Dye-dispersing ZnO precursor gel films were prepared on indium tin oxide electrodes from a zinc acetate solution containing eosin Y by dip-coating, steam treatment, and then heating at a low temperature. The electronic interaction between the dye and zinc in the dye-dispersing gel films were investigated by spectroscopic and electrochemical measurements. A photocurrent was observed in the dye-dispersing gel electrodes before the steam treatment. The photocurrent value increased by the steam treatment and heating due to crystallization of the gel and removal of organic impurities. The dye molecules existed between the interlayers of the layered zinc hydroxide coexisting with the ZnO. The photoexcited electron in the dye should be injected into the ZnO conduction band via the layered zinc hydroxide. The value increased with an increase in the dye content even though the ZnO crystallinity decreased. The dye–zinc interaction, i.e., the complex formation and photoinduced electron injection, played an important role in the electron transport and photoelectric conversion.

Keywords: ZnO, eosin Y, wet process, steam treatment, dye–zinc interaction, photoinduced electron injection

Introduction

Organic−inorganic composites are promising and interesting materials for use in photofunctional devices such as light emitting [1–3], light harvesting [4,5], solar energy conversion [6–8], etc., which effectively utilize the photoactive properties of the organic dye molecules. Wet processes, such as the sol–gel method, are useful methods to prepare inorganic thin films containing organic compounds because they easily form nanocrystalline materials [9–13]. In the sol–gel matrices, the dye molecules having a high photofunction can be encapsulated in the small pores of the inorganic matrices [14–19]. The compounds in such materials exhibit a more efficient light harvesting and fluorescence because they are finely dispersed in the amorphous or nanosized crystalline matrices compared to the conventional dye-adsorbing materials [20–23]. Therefore, it is expected that such films exhibit a higher function, stability, and performance in various applications.

The organic dye-dispersing titania gel is suited for the dye–titania complex formation because the dye molecules with carbonyl and/or carboxyl groups are encapsulated in the narrow spaces of the gel [20–26]. The xanthene dye-dispersing titania gel was prepared without heating from a titanium alkoxide sol containing the dye molecules by the sol–gel method [27–31]. Xanthene dyes as laser dyes are available materials for utilizing photoenergy due to their high absorption and fluorescence efficiencies in various visible light regions [32]. It was reported that the hydrothermal treatment of a dye-dispersing

amorphous titania film remarkably improved the photoelectric conversion efficiency due to not only its crystallization but also the dye–titanium complex formation [20–31].

ZnO is an interesting material and has been used in various applications, for example, in white pigment, cosmetics, or electrochemical devices. In recent years, ZnO has been investigated as a varistor resistor and transistor because it has a semiconductor property [33–35]. Dye-dispersing ZnO films as well as normal ZnO films can be prepared by wet processes at a lower temperature than the titania films [36–38]. Furthermore, ZnO has a higher carrier mobility in the bulk than titania [34]. ZnO is expected to more strongly bond to the carbonyl oxygen of the dye molecules than titania due to its higher electron affinity [39].

In this study, the dye-dispersing ZnO precursor films were prepared on indium tin oxide (ITO) electrodes from a zinc acetate solution containing the dye by dip-coating, steam treatment, and then heating at a low temperature. The dye–zinc interaction, i.e., the complex formation, improves the photoinduced electron injection and electron transport, which concern some radical or intermediate species. Our study can potentially contribute to new knowledge of the physicochemical properties of such nanocomposites and their applications in nano-sized electronic devices. Eosin Y, one of the xanthene dyes, was used as the photosensitizer. This dye can more strongly interact with the zinc species although it weakly interacted with the titanium species in a previous study [20,23]. The photoinduced

electron transfer and transport properties of the dye-dispersing ZnO precursor films were investigated by spectroscopic and electrochemical measurements in order to evaluate the electronic interaction between the dye and zinc compared to the dye-dispersing titania systems.

Experimental

Materials

Zinc acetate dihydrate ($Zn(CH_3CO_2)_2 \cdot 2H_2O$), methanol, eosin Y, hydrochloric acid, sodium hydroxide, diethylene glycol, iodine, and lithium iodide (Wako Pure Chemical Industries, S or reagent grade) were used without further purification. Water was ion-exchanged and distilled by a distiller (Yamato WG23). Glass plates (Matsumani S1126) and those coated with the ITO transparent electrode (AGC Fabritech) were soaked in hydrochloric acid (1.0 mol dm^{-3}) for 2 h, then rinsed with water. The electrolyte used for the electrical measurements consisted of a diethylene glycol solution of iodine (5.0×10^{-2} mol dm^{-3}) and lithium iodide (0.50 mol dm^{-3}).

Preparation of electrodes

The precursor solutions were prepared by mixing 1.31 g of $Zn(CH_3CO_2)_2 \cdot 2H_2O$, 30.0 cm^3 of methanol, and 0.60 cm^3 of a 1.0 mol dm^{-3} sodium hydroxide aqueous solution. These solutions were labeled SG-0. Eosin Y was dissolved in the SG-0 in which its concentration

was 1.0×10^{-3}, 5.0×10^{-3}, and 1.0×10^{-2} mol dm^{-3} and these systems were labeled SG-0.1, SG-0.5, and SG-1, respectively. The dip-coated thin films were prepared from these systems.

In order to prepare the electrode samples coated with the crystalline titania, the glass plates with the ITO transparent electrode were dip-coated in the dye-free system, SG-0, and then heated at 450 ºC for 30 min. These electrodes were labeled E-0. Furthermore, the working electrodes were prepared in which the E-0 was dip-coated with SG-0, SG-0.1, SG-0.5, or SG-1. These working electrodes were labeled WE-0, WE-0.1, WE-0.5, and WE-1, respectively. The glass plates without the ITO were also coated with SG-0, SG-0.1, SG-0.5, or SG-1 in order to obtain their X-ray diffraction (XRD) patterns and spectroscopic information. These film samples were labeled F-0, F-0.1, F-0.5, and F-1, respectively.

The steam-treatment effects on the XRD patterns and spectroscopic and photocurrent properties of the samples were investigated. Water was heated at 100 ºC and the electrode and XRD samples were exposed to its steam for 20, 40, and 60 min. The steam pressure was about 100 kPa. The steam-treated samples were additionally labeled "-20S, -40S, and -60S", i.e. WE-0-20S, WE-0-40S, and WE-0-60S. The samples steam-treated for 20 and 60 min were heated at 200 ºC for 120 min and additionally labeled "-H", i.e. WE-1-20S-H and WE-1-60S-H.

Measurements

Surface micromorphology of the samples was observed using a field emission scanning electron microscope (FE-SEM; Hitachi SU8000). The crystalline phase of the film samples was determined using an X-ray diffractometer (Rigaku SmartLab). The UV–visible absorption spectra of the prepared film samples were observed using a spectrophotometer (Shimadzu UV-3510). The amounts of the dyes present in the electrode samples were estimated from the absorption spectra of the dye eluted by the 0.1 mol dm^{-3} sodium hydroxide aqueous solution.

The dye powders and the flakes of the dye-dispersing film samples were pressed in KBr pellets and their IR spectra were obtained using a Fourier transform infrared (FTIR) spectrophotometer (Shimadzu IRPrestige-21).

The iodine-based electrolyte was allowed to soak into the space between the electrode sample and the counter Pt electrode. Monochromatic light at each wavelength obtained from the fluorescence spectrophotometer using a 150-W Xe short arc lamp (Ushio UXL-155) was irradiated on the electrodes for the spectroscopic measurements. During the light irradiation, the short circuit currents of the electrodes were measured by a digital multimeter (ADCMT 7461A). The current density–applied voltage (*J*–*V*) curves of the electrodes were measured by a potentiostat (Hokuto Denko HSV-100) during the visible light irradiation at a wavelength longer than 400 nm emitted by the 150-W Xe short arc lamp using a sharp cut filter. The intensity at each wavelength of the light source was obtained using a power

meter (Molectron PM500A) in order to estimate the incident photon-to-current conversion efficiency (IPCE) and quantum efficiency for the photocurrent from the excited dye in the electrode samples. The visible absorbance of the present electrode samples was lower than 1.0 which was sufficient to measure the number of absorbed photons in order to calculate the quantum efficiency.

Results and discussion

Structure of the films

Figure 1 shows the SEM images of the surface of the electrode samples without and with the dye prepared from SG-0 and SG-1, respectively. The ZnO precursor films consisted of 10–30 nm-sized spherical particles. The particle shape was not angular and slightly changed by the steam treatment and heating under the present conditions. They did not seem to be ZnO crystalline particles, which generally consist of hexagonal columns.

(Figure 1)

Figure 2 shows the XRD patterns of the films prepared from SG-0 and SG-1. The untreated films without the dye exhibited broad peaks at ca. 12° and 18°. The former can be assigned to the (200) plane of the raw material, $Zn(CH_3CO_2)_2 \cdot 2H_2O$ [40]. The former and latter can also be assigned to the (110) and (−112) planes of $NaCH_3CO_2 \cdot 3H_2O$ by neutralization of the raw materials [41]. The steam treatment of the dye-free film induced

the formation of the layered zinc hydroxide salt and ZnO, which exhibited broad peaks at ca. 6° assigned to the (001) plane of $Zn_5(OH)_8(CH_3CO_2)_2 \cdot 2H_2O$ and at 31.7°, 34.3°, and 36.2° assigned to the (100), (002), and (101) planes of the wurtzite-type ZnO, respectively [36–38,42–44]. The XRD pattern was not significantly changed by heating at 200 °C. On the other hand, the untreated dye-containing film was amorphous. A peak was observed at 8.9° after the steam treatment. This peak can be assigned to the (002) plane of the layered zinc hydroxide containing eosin Y between its interlayers [45–47]. It has been reported that the layered zinc hydroxide salts can exchange the anions between the interlayers for some anions [42]. Figure S1 shows XRD patterns of the films prepared from SG-0, SG-0.5, and SG-1, which were steam-treated for 40 min (Supporting information). The (002) peak was shifted to the lower direction with an increase in the dye content. The interlayer space was suggested to be expanded by the ion exchange of the larger ions. Weak ZnO peaks were also observed in the films after the steam treatment and heating. A previous study indicated that the organic dye molecules strongly interacted with metal and inhibited the crystallization of the metal oxide precursor [28,48].

(Figure 2)

The average ZnO crystallite sizes of the samples were estimated from the full width at half-maximum of the (101) peak using Scherrer's equation as shown in Table 1. The sizes of the dye-containing samples were smaller than those of the dye-free samples. The

crystallite sizes did not correspond to the particle sizes seen in the SEM images. This fact indicated that the particles were secondary particles consisting of crystallite aggregates. It is suggested that the dye molecules suppressed the crystal growth of ZnO due to the interaction between the dye and zinc, i.e., complex formation. On the other hand, such dye molecules slightly affected the crystallization of the titania gel [20,28].

(Table 1)

Figure 3 shows the FTIR spectra of the films prepared from SG-0 and SG-1. Eosin Y exhibits its main peaks at 1554, 1456, and 1350 cm^{-1} assigned to the COO^- anti-symmetric, quinone-like C=O, and COO^- symmetric stretching vibrations, respectively [20,49]. The acetate ion of zinc acetate exhibited peaks at 1560, 1450−1390, and 680 cm^{-1} assigned to the COO^- anti-symmetric stretching, symmetric stretching, and out-of-plane bending vibrations, respectively [50–53]. In the dye-free films, the intensity of the acetate peaks decreased by the steam treatment, and, furthermore, they disappeared by heating due to their evaporation. The peak wavenumber of the COO^- anti-symmetric and symmetric stretchings was shifted to the higher and lower directions, respectively, by the steam treatment. This result indicated that the interaction between some acetate and zinc was enhanced by the hot water molecules although most of the acetate evaporated [20,24,26]. Acetate existing between the zinc hydroxide interlayers was difficult to remove. On the other hand, the eosin Y remained in the films although the acetate was removed. The quinone-like C=O band was shifted to the

lower direction by the steam treatment and heating in addition to the shift in the acetate bands. This result indicated the enhancement of the dye–zinc interaction, i.e., complex formation between the zinc hydroxide interlayers instead of the interaction between the acetate and zinc. In our previous study, such shift was also observed in the fluorescein-dispersing titania due to the fluorescein–titania complex formation [20,24], whereas eosin Y weakly interacted with the titanium species due to its lower electron affinity than zinc [20,23,39].

(Figure 3)

Interaction between the dye and zinc

Figure 4 shows the UV–Vis absorption spectra of the dye-containing films at a different concentration. The absorbance was confirmed to be proportional to the dye content by quantification of the eluted dye molecules. The untreated films have a peak at 530 nm, which is assigned to the dianion species of eosin Y and longer than its peak observed in water due to the ionic interaction with the metrics surface [54]. The absorbance values of the films were proportional to the dye concentration before the treatment and decreased with an increase in the steam treatment time. This decrease is due to desorption of the dye into the water phase. The values reached about half after the 20-min treatment. The values slightly changed after the 60-min treatment, although they decreased to lower than one-third in the previous titania system [20,26]. The peaks were shifted in the longer wavelength direction by the steam treatment, indicating the possibility of the dye–zinc complex formation.

The steam treatment enhanced the fluorescein dye–titania surface complex formation in our previous study [20,24,26]. However, eosin Y weakly interacted with the titanium species even after steam treatment, because the oxygen atoms of its carboxyl and quinone-like groups are less nucleophilic than those of fluorescein and more difficult to form the coordination complex with metal species [20,23]. In the present systems, eosin Y can interact with the zinc between the zinc hydroxide interlayers.

(Figure 4)

Figure 5 shows the IPCE spectra of the electrode samples in the UV and visible ranges for the ZnO and eosin Y absorptions, respectively. The photocurrent observed in the UV and visible ranges originated from the electrons generated upon excitation of the ZnO and eosin Y. The excited electrons in eosin Y were injected into the conduction band of ZnO. The peak wavelength in the visible range was 530 nm for all the samples, although the absorption peaks of the steam-treated and heated samples were observed at 535 nm. This is because the interaction was somewhat weakened in the electrolyte solution during the photoelectrochemical measurements, whereas the eosin Y was suggested to form a rigid dye–zinc complex in the dry electrode samples. The IPCE values in the UV and visible ranges were increased by the steam treatment and heating due to the ZnO production and removal of the organic impurities based on the XRD and FTIR analyses. Especially, the initial 20-min steam treatment was the most effective process. The values decreased during the treatment

of the dye-dispersing electrodes for more than 20 min. The IPCE values also increased with an increase in the dye concentration. These results indicated that the photoinduced electron injection and transport were improved by the formation of the dense ZnO conduction band, effective connection of the ZnO particles, and the dye–zinc interaction instead of the interaction between the acetate and zinc.

(Figure 5)

The *J*–*V* curves of the dye-free and dye-containing electrodes were observed during the UV and visible irradiations, respectively, as shown in Figure 6. The short circuit current density values corresponded to the IPCE values. The increase in the open circuit voltage values was caused by the suppression of the back electron transfer due to the increase in the crystallinity. In the dye-free electrodes, the short circuit current and open circuit voltage value increased with an increase in the steam treatment time and further increased by heating. In the dye-containing electrodes, such increases were significantly observed during the initial 20-min treatment. The values decreased during the treatment of more than 20 min. This trend can be more clearly seen in the samples containing a higher amount of eosin Y because the dye molecules, i.e., the dye–zinc complexes, inhibited the crystallization of ZnO. A reason for the decrease is suggested, in that the bonds between the crystalline particles were weakened by hydrolysis based on the XRD analysis results as seen in the previous titania systems [20].

(Figure 6)

Figure 7 shows the quantum efficiencies of the photoelectric conversion at 350 and 530 nm upon the ZnO and eosin Y excitation, respectively, for the electrodes. In the dye-free electrodes, the quantum efficiency was increased by the steam treatment and heating. On the other hand, the efficiency was significantly increased by the initial 20-min treatment, but slightly decreased by further treatment. This phenomenon did not correspond to the result observed in the fluorescein-dispersing titania systems, in which the short circuit current, open circuit voltage, and quantum efficiency increased with an increase in the steam treatment time due to the dye–titania complex formation [20]. The present decrease is suggested to be due to the dye molecules existing between the interlayers of the layered zinc hydroxide. Figure S2 shows the FTIR spectra (4000–2600 cm^{-1}) of the films prepared from SG-1 (Supporting information). The intensity of the OH stretching band at around 3400 cm^{-1} assigned to the intercalated water increased with the steam treatment time and decreased by heating. The water molecules deactivated the dye sensitization because they were oxidized instead of the dye molecules during the photocatalytic process. The dye molecules indirectly interacted with ZnO, i.e., the electron should be injected into the ZnO conduction band via the layered zinc hydroxide. The quantum efficiency increased during heating by removal of the acetate and water from the electrode sample, i.e., enhancement of the dye–zinc interaction, rather than by an increase in the crystallinity. This is due to the effective increases in the

efficiencies of the electron injection and transport. The quantum efficiency was very low in the present electrodes, because the prepared ZnO even without the dye has a significant number of defects. The efficiency of the electron injection from the dye molecule to the ZnO was estimated by dividing the quantum efficiency upon the dye excitation by that upon the ZnO excitation. The values were 20−40 % for the steam-treated samples and 50−75 % for the heated samples, which mainly depended on the quantum efficiency upon the dye excitation, as shown in Figure 7.

(Figure 7)

Figures S3 and S4 show the UV–Vis absorption and IPCE spectra of the electrode prepared from SG-0 which was steam-treated for 60-min, WE-0-60S, and then eosin Y-adsorbed. The eosin Y molecules should be weakly adsorbed on the ZnO particle surface in WE-0-60S with the small amount of zinc hydroxide. The quantum efficiencies at 350 and 530 nm estimated from the absorption and IPCE values were 8.3 % and 0.20 %, respectively. The electron injection efficiency was 2.5 %. The quantum efficiency at 530 nm and electron injection efficiency were significantly lower than those of the electrodes having the dye molecules between the interlayers of the layered zinc hydroxide. These results supported that the dye–zinc interaction effectively enhanced the electron injection into the ZnO conduction band via the layered zinc hydroxide.

Figure 8 shows the IPCE values at 350 nm and crystallite sizes of the electrodes prepared

from SG-0 and SG-1. The IPCE value in the UV range due to the ZnO absorption increased with an increase in the crystallite size because the crystallinity was related to the electronic conductivity. Figure 9 shows the IPCE and absorbance values at 530 nm due to the eosin Y absorption and absorbance at 680 cm^{-1} due to acetate for the samples prepared from SG-1. The IPCE value increased with an increase in the steam treatment time and further increased by heating. The amount of acetate in the samples decreased with an increase in the IPCE value, indicating that the photoelectric conversion efficiency was improved by the removal of acetate and enhancement of the dye–zinc interaction. The electron transport efficiency was enhanced by increasing the ZnO particle connection without any acetate.

(Figures 8 and 9)

Conclusions

The dye-dispersing ZnO precursor films were prepared on ITO electrodes from a zinc acetate solution containing the dye by dip-coating, steam treatment, and then heating at a low temperature. The photoinduced electron transfer and transport properties of the dye-dispersing films were investigated by spectroscopic and electrochemical measurements in order to examine the electronic interaction between the dye and zinc compared to the dye-dispersing titania systems. The dye molecules existed between the interlayers of the

layered zinc hydroxide coexisting with the ZnO. The photoexcited electron in the dye should be injected into the ZnO conduction band via the layered zinc hydroxide. A photocurrent was observed in the dye-dispersing gel electrodes before the steam treatment. The photoelectric conversion efficiency was increased by the steam treatment and heating due to crystallization of the gel and removal of the organic impurities in it. This value increased with an increase in the dye content even though the ZnO crystallinity decreased. The photoinduced electron injection efficiency was improved by removal of the acetate and enhancement of the dye–zinc interaction, i.e., dye–zinc complex formation. The electron transport efficiency was enhanced by increasing the ZnO particle connection without any acetate present.

Acknowledgments

This work has been supported by JSPS KAKENHI Grant Number 24550153.

References

1 K. Chondroudis, D. B. Mitzi, Chem. Mater. **11**, 3028 (1999)

2 F. Li, Z. Chen, W. Wei, Q. Gong, Org. Electron. **6**, 237 (2005)

3 Y. Kajiwara, A. Nagai, K. Tanaka, Y. Chujo, J. Mater. Chem. C **1**, 4437 (2013)

4 Y. Maegawa, N. Mizoshita, T. Tani, S. Inagaki, J. Mater. Chem. **20**, 4399 (2010)

5 K. Y. Pu, K. Li, B. Liu, Adv. Mater. **22**, 643 (2010)

6 M. Grätzel, J. Photochem. Photobiol. C **4**, 145 (2003)

7 D. El Mekkawi, M. S. A. Abdel-Mottaleb, Int. J. Photoenergy **7**, 95 (2005)

8 G. D. Sharma, P. Balraju, M. Kumar, M. S. Roy, Mater. Sci. Eng. B **162,** 32 (2009)

9 H. Dislich, Angew. Chem. Int. Ed. Engl. **10**, 363 (1971)

10 H. Dislich, J. Non Cryst. Solids **57**, 371 (1983)

11 C. J. Brinker, G. W. Scherer, *Sol–gel science: the physics and chemistry of sol–gel processing* (Academic Press, San Diego, 1990)

12 C. J. Brinker, G. C. Frye, A. J. Hurd, C. S. Ashley, Thin Solid Films **201**, 97 (1991)

13 C. J. Brinker, A. J. Hurd, G. C. Frye, P. R. Schunk, C. S. Ashley, J. Ceram. Soc. Jpn. **99**, 862 (1991)

14 D. Avnir, D. Levy, R. Reisfeld, J. Phys. Chem. **88**, 5956 (1984)

15 R. Reisfeld, R. Zusman, Y. Cohen, M. Eyal, Chem. Phys. Lett. **147**, 142 (1988)

16 T. Fujii, A. Ishii, M. Anpo, J. Photochem. Photobiol. A **54**, 231 (1990)

17 U. Narang, F. V. Bright, P. N. Prasad, Appl. Spectrosc. **47**, 229 (1993)

18 H. Nishikiori, T. Fujii, J. Phys. Chem. B **101**, 3680 (1997)

19 H. Nishikiori, N. Tanaka, Y. Minami, A. Katsuki, T. Fujii, J. Photochem. Photobiol. A **212**, 62 (2010)

20 H. Nishikiori, Y. Uesugi, S. Takami, R. A. Setiawan, T. Fujii, W. Qian, M. A. El-Sayed, J.

Phys. Chem. C **115**, 2880 (2011)

21 H. Nishikiori, Y. Uesugi, R. A. Setiawan, T. Fujii, W. Qian, M. A. El-Sayed, J. Phys. Chem. C **116**, 4848 (2012)

22 H. Nishikiori, R. A. Setiawan, K. Miyashita, K. Teshima, T. Fujii, Catal. Sci. Technol. **3**, 1512 (2013)

23 H. Nishikiori, R. A. Setiawan, S. Kawamoto, S. Takagi, K. Teshima, T. Fujii, Catal. Sci. Technol. **3**, 2786 (2013)

24 R. A. Setiawan, H. Nishikiori, Y. Uesugi, K. Miyashita, M. A. El-Sayed, T. Fujii, J. Phys. Chem. C **117**, 10308 (2013)

25 R. A. Setiawan, H. Nishikiori, N. Tanaka, T. Fujii, Chem. Lett. **42**, 1391 (2013)

26 H. Nishikiori, R. A. Setiawan, K. Miyashita, K. Teshima, T. Fujii, Photochem. Photobiol. **90**, 747 (2014).

27 H. Nishikiori, N. Tanaka, T. Kitsui, T. Fujii, Photocurrent observed in dye-doped titania gel, J. Photochem. Photobiol. A **179**, 125 (2006)

28 T. Kitsui, H. Nishikiori, N. Tanaka, T. Fujii, J. Photochem. Photobiol. A **192**, 220 (2006)

29 H. Nishikiori, W. Qian, M. A. El-Sayed, N. Tanaka, T. Fujii, J. Phys. Chem. C **111**, 9008 (2007)

30 H. Nishikiori, Y. Uesugi, N. Tanaka, T. Fujii, J. Photochem. Photobiol. A **207**, 204 (2009)

31 H. Nishikiori, R. A. Setiawan, K. Miyamoto, G. Sukmono, Y. Uesugi, K. Teshima, T.

Fujii, RSC Adv. **2**, 4258 (2012)

32 Maeda, *Laser dyes: properties of organic compounds for dye lasers* (Academic Press, Tokyo, 1984)

33 L. Spanhel, M. A. Anderson, J. Am. Chem. Soc. **113**, 2826 (1991)

34 J. A. Anta, E. Guillén, R. Tena-Zaera, J. Phys. Chem. C **116**, 11413 (2012)

35 S. Sakthivel, B. Neppolian, M.V. Shankar, B. Arabindoo, M. Palanichamy, V. Murugesan, Sol. Energy Mater. Sol. Cells **77**, 65 (2003)

36 L. Poul, N. Jouini, F. Fiévet, Chem. Mater. **12**, 3123 (2000)

37 E. Hosono, S. Fujihara, T. Kimura, Electrochim. Acta **49**, 2287 (2004)

38 A. Tarat, R. Majithia, R. A. Brown, M. W. Penny, K. E. Meissner, T. G. G. Maffeis, Surf. Sci. **606**, 715 (2012)

39 D. R. Lide (ed.), *CRC Handbook of Chemistry and Physics,* 85th edn. (CRC Press, Boca Raton, 2004) pp. 10-183–10-184

40 ICDD PDF 33-1464

41 ICDD PDF 29-1159

42 H. Morioka, H. Tagaya, J.-I. Kadokawa, K. Chiba, J. Mater. Sci. Lett. **18**, 995 (1999)

43 E. Hosono, T. Tokunaga, S. Ueno, Y. Oaki, H. Imai, H. Zhou, S. Fujihara, J. Ceram. Soc. Jpn. **120**, 171 (2012)

44 A. Moezzi, M. B. Cortie, R. Shimmon, A. M. McDonagh, Eur. J. Inorg. Chem. **2013**,

5133 (2013)

45 G. Guadalupe C. Arizaga, A. S. Mangrich, J. E. F. C. Gardolinski, F. Wypych, Gregorio, J. Colloid Interface Sci. **320**, 168 (2008)

46 A. F. Abdul Latip, M. Z. Hussein, J. Stanslas, C. C. Wong, R. Adnan, Chem. Cent. J. **7,** 119 (2013)

47 A. Zimmermann, S. Jaerger, S. F. Zawadzki, F. Wypych, J. Polym. Res. **20,** 224 (2013)

48 H. Nishikiori, K. Todoroki, D. Natori, R. A.Setiawan, K. Miyashita, T. Fujii, Chem. Lett. **42**, 556 (2013)

49 L. Wang, A. Roitberg, C. Meuse, A. K. Gaigalas, Spectrochem. Acta. A **57**, 1781 (2001)

50 M. A. Hasan, M. I. Zaki, L. Pasupulety, Appl. Catal. A **243**, 81 (2003)

51 S.M. York, S. H aq, K.V. Kilway, J.M. Phillips, F.M. Leibsle, Surf. Sci. **522**, 34 (2003)

52 J. J. Max, C. Chapados, J. Phys. Chem. A **108**, 3324 (2004)

53 A. Brücknera, U. Bentrup, M. Fait, B. Kubias, Catal. Today **99**, 123 (2005)

54 N. O. Mchedlov-Petrossyan, V. N. Kleshchevnikova, J. Chem. Soc. Faraday Trans. **90**, 629 (1994)

Table 1 Average ZnO crystallite sizes (/ nm) of the samples estimated from the full width at half maximum of the (101) peak in the XRD patterns using Scherrer's equation

F-0-20S	F-0-40S	F-0-60S	F-0-20S-H	F-0-60S-H
14.7	15.5	16.1	14.7	16.7
F-1-20S	F-1-40S	F1-60S	F-1-20S-H	F-1-60S-H
7.61	7.74	7.89	7.74	7.97

Figure captions

Fig. 1 SEM images of surface of (a) WE-0, (b) WE-0-60S, (c) WE-0-60S-H, (d) WE-1, (e) WE-1-60S, and (f) WE-60S-H

Fig. 2 XRD patterns of the films prepared from SG-*n*; (a) *n* = 0 and (b) *n* = 1, (1) F-*n*, (2) F-*n*-20S, (3) F-*n*-40S, (4) F-*n*-60S, (5) F-*n*-20S-H, and (6) F-*n*-60S-H. The peaks are assigned to ZnO (●), $Zn_5(OH)_8(CH_3CO_2)_2 \cdot 2H_2O$ (♦), $Zn(CH_3CO_2)_2 \cdot 2H_2O$ (▼), $NaCH_3CO_2 \cdot 3H_2O$ (▲), and zinc hydroxide containing eosin Y(■)

Fig. 3 FTIR spectra of the films prepared from SG-*n*; (a) *n* = 0 and (b) *n* = 1, (1) F-*n*, (2) F-*n*-20S, (3) F-*n*-40S, (4) F-*n*-60S, (5) F-*n*-20S-H, and (6) F-*n*-60S-H. The spectra of zinc acetate and eosin Y powers are also shown

Fig. 4 UV–Vis absorption spectra of the films prepared from SG-*n*; (a) *n* = 0.1, (b) *n* = 0.5, and (c) *n* = 1

Fig. 5 IPCE spectra of the electrodes prepared from SG-*n*; (a) *n* = 0, (b) *n* = 0.1, (c) *n* = 0.5, and (d) *n* = 1

Fig. 6 *J*−*V* curves of the electrodes prepared from SG-*n*; (a) *n* = 0, (b) *n* = 0.1, (c) *n* = 0.5, and (d) *n* = 1. The measurement was conducted during the UV irradiation, *n* = 0 and visible irradiation, *n* = 0.1, 0.5, and 1

Fig. 7 Quantum efficiencies of photoelectric conversion for the electrodes prepared from

SG-*n*; (a) *n* = 0, (b) *n* = 0.1, (c) *n* = 0.5, and (d) *n* = 1. The efficiencies were obtained at 350 and 530 nm. The electron injection efficiencies were also estimated for the dye-containing electrodes

Fig. 8 Relationship between IPCE values at 350 nm and average crystallite sizes for the samples prepared from SG-*n*; *n* = 0 and *n* = 1

Fig. 9 Relationship between IPCE values at 530 nm and absorbance values at 530 nm and 680 cm^{-1} for the samples prepared from SG-1

Fig. 1

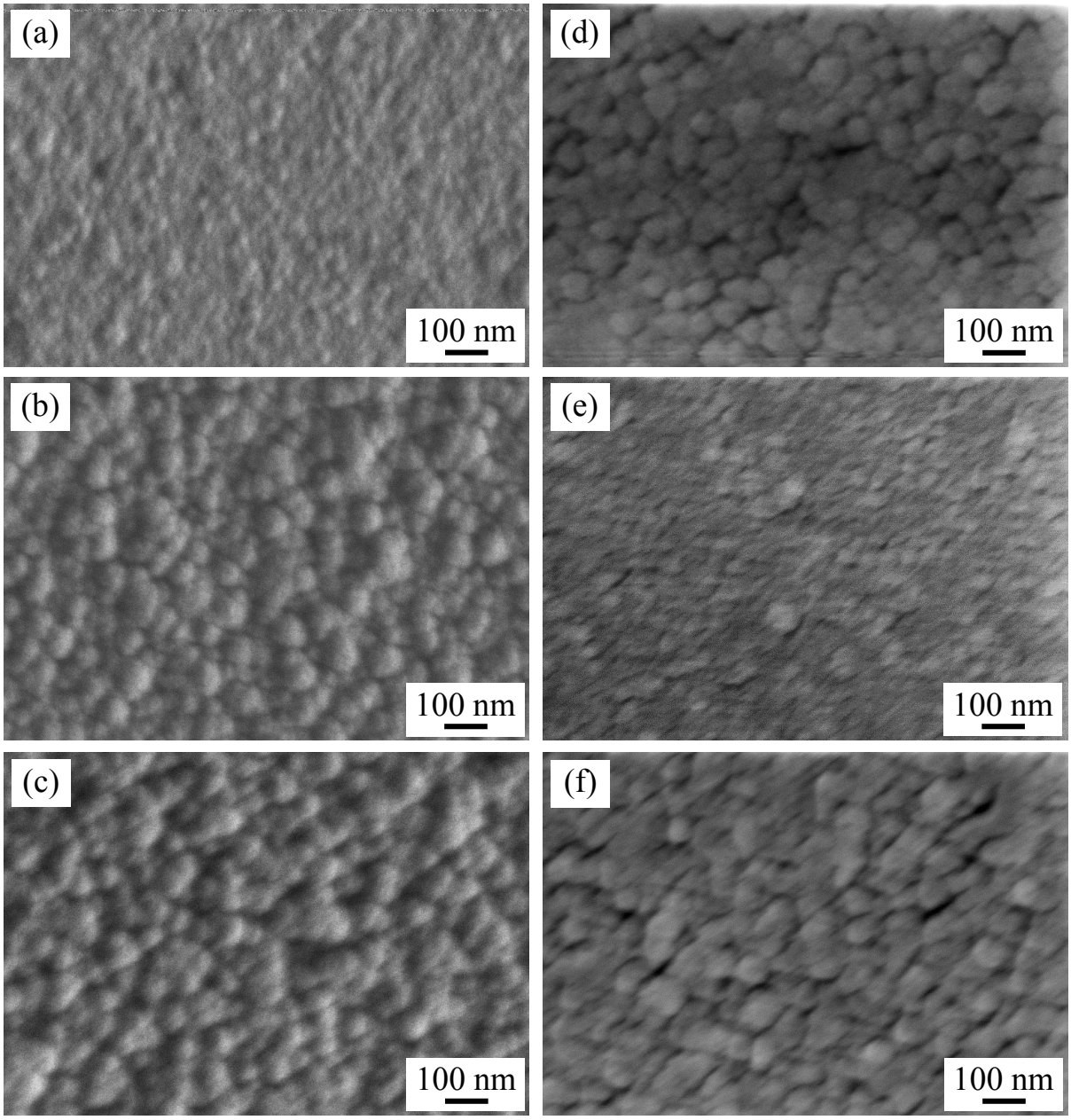

Fig. 2

(a)

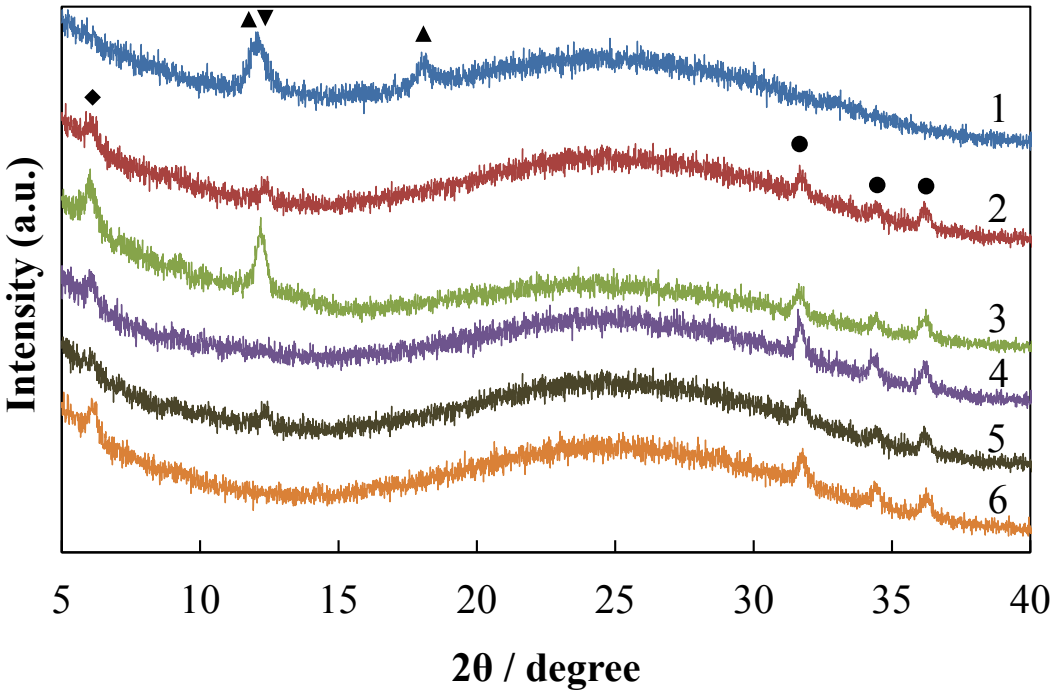
Intensity (a.u.)
1
2
3
4
5
6
5
10
15
20
25
30
35
40
2θ / degree

(b)

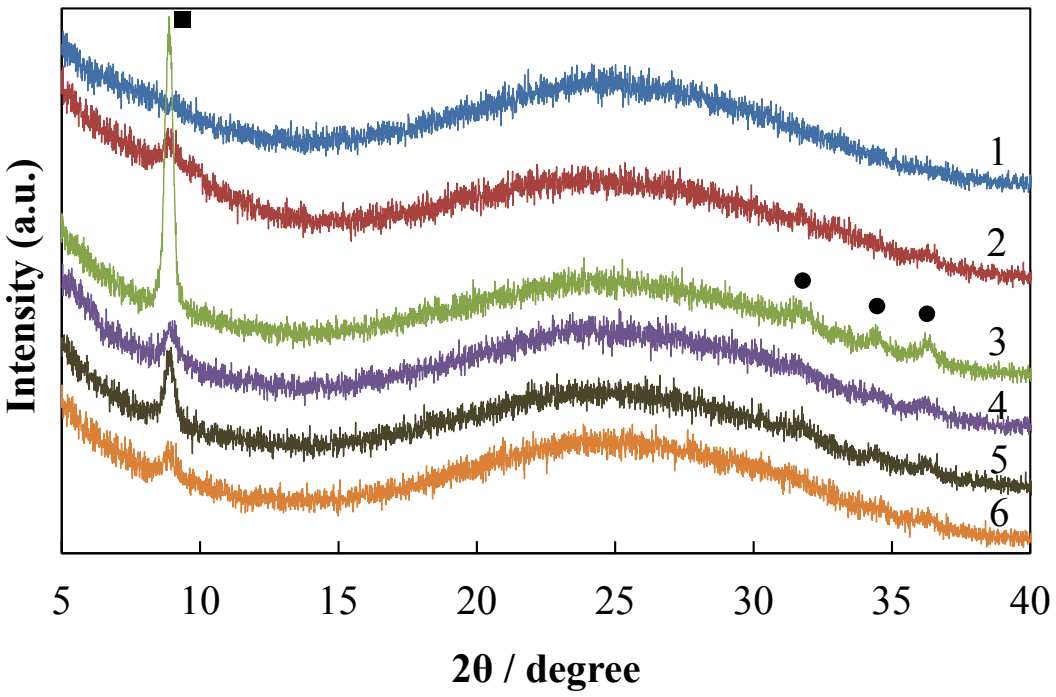
Intensity (a.u.)
1
2
3
4
5
6
5
10
15
20
25
30
35
40
2θ / degree

Fig.3

(a)

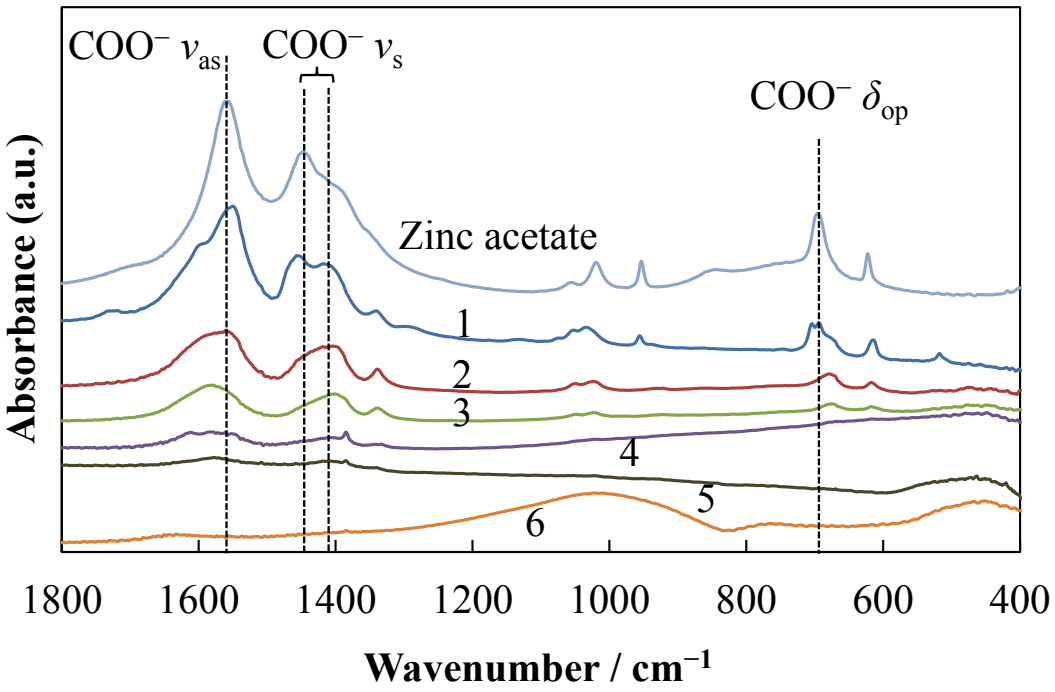
COO⁻ v_{as}
COO⁻ v_s
COO⁻ δ_{op}
Zinc acetate
1
2
3
4
5
6
Absorbance (a.u.)
1800
1600
1400
1200
1000
800
600
400
Wavenumber / cm⁻¹

(b)

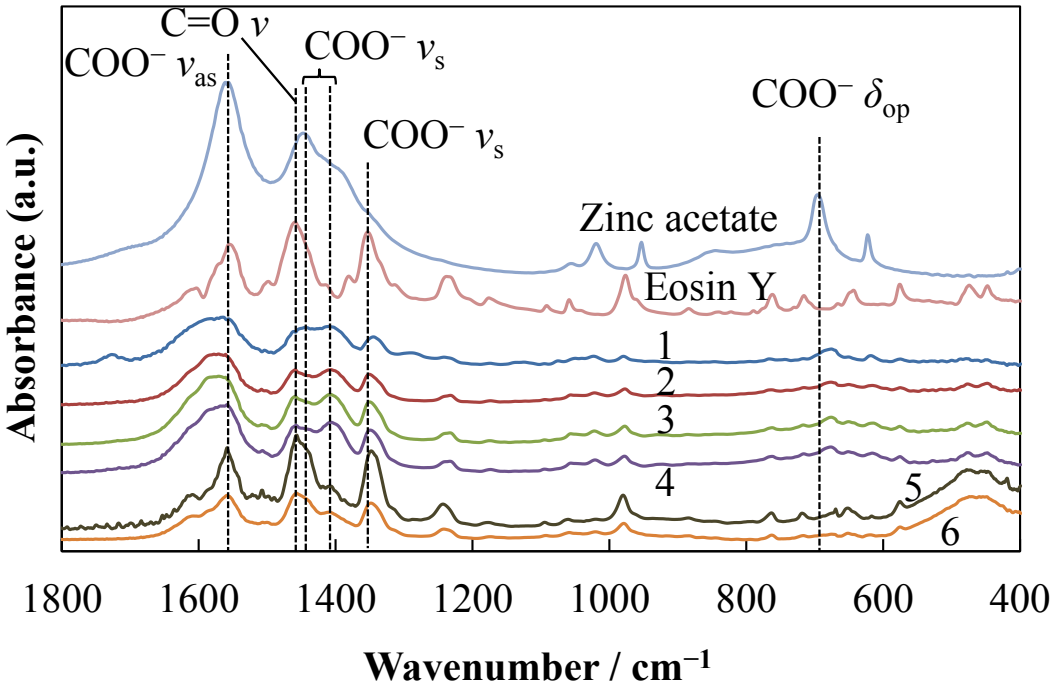
C=O v
COO⁻ v_{as}
COO⁻ v_s
COO⁻ v_s
COO⁻ δ_{op}
Zinc acetate
Eosin Y
1
2
3
4
5
6
Absorbance (a.u.)
1800
1600
1400
1200
1000
800
600
400
Wavenumber / cm⁻¹

Fig. 4

(a)

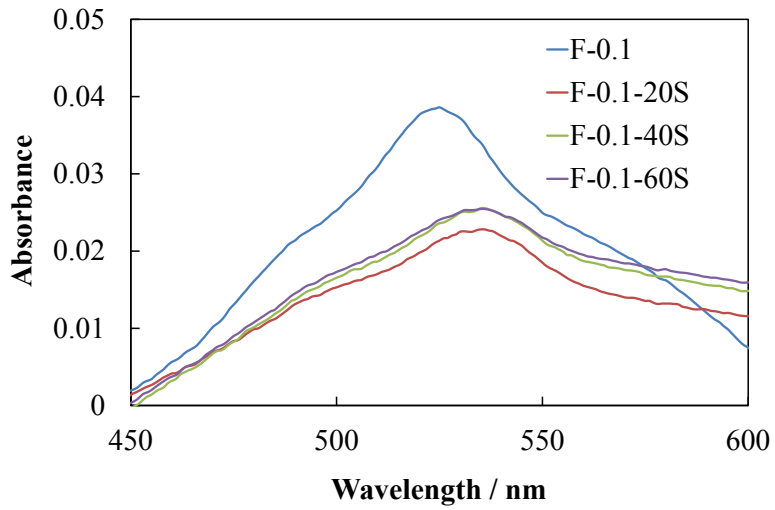
0.05
0.04
0.03
0.02
0.01
0
Absorbance
450
500
550
600
Wavelength / nm
F-0.1
F-0.1-20S
F-0.1-40S
F-0.1-60S

(b)

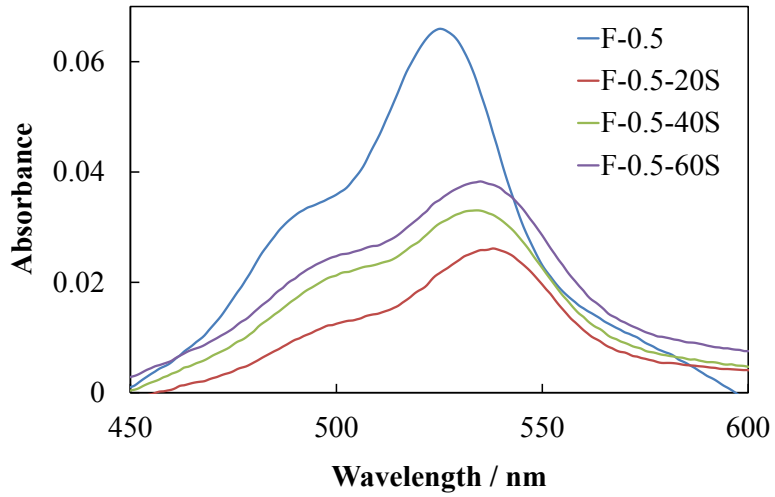
0.06
0.04
0.02
0
Absorbance
450
500
550
600
Wavelength / nm
F-0.5
F-0.5-20S
F-0.5-40S
F-0.5-60S

(c)

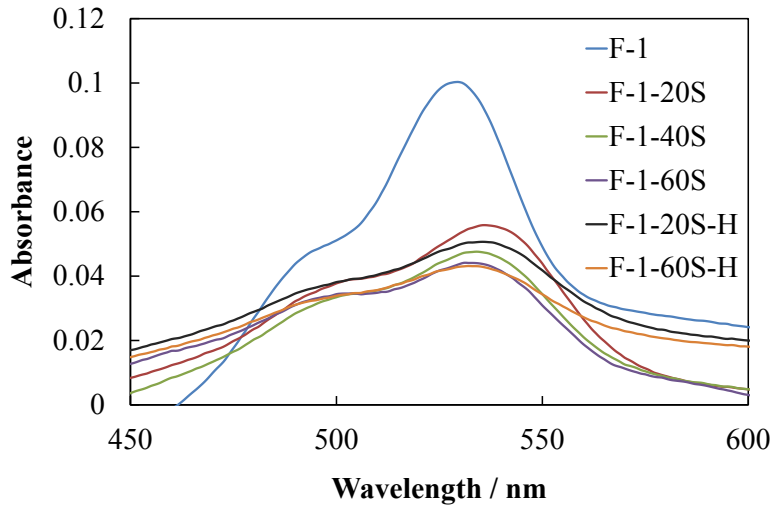
0.12
0.1
0.08
0.06
0.04
0.02
0
Absorbance
450
500
550
600
Wavelength / nm
F-1
F-1-20S
F-1-40S
F-1-60S
F-1-20S-H
F-1-60S-H

Fig. 5

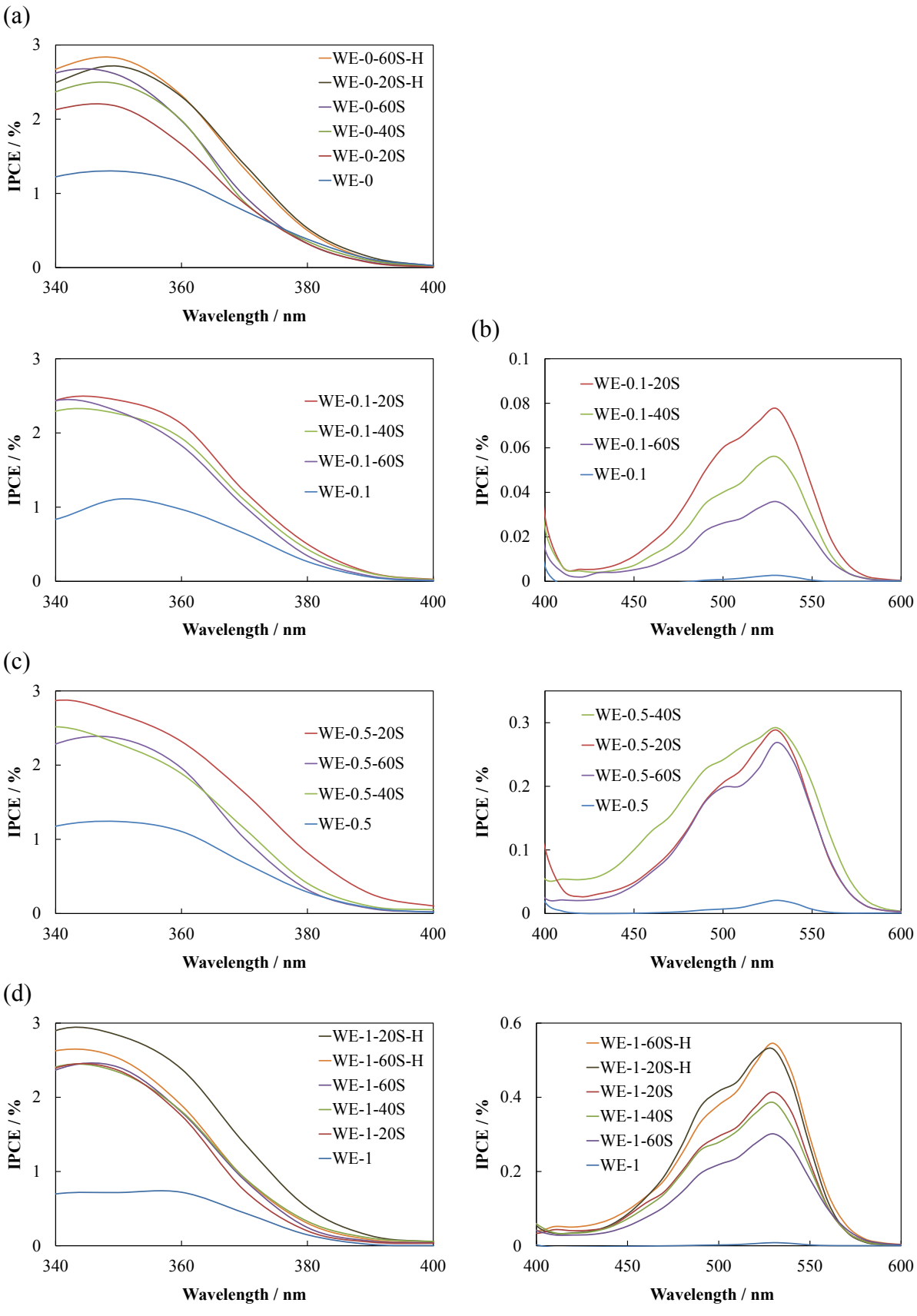
(a)
WE-0-60S-H
WE-0-20S-H
WE-0-60S
WE-0-40S
WE-0-20S
WE-0
IPCE / %
Wavelength / nm
(b)
WE-0.1-20S
WE-0.1-40S
WE-0.1-60S
WE-0.1
IPCE / %
Wavelength / nm
(c)
WE-0.5-20S
WE-0.5-60S
WE-0.5-40S
WE-0.5
IPCE / %
Wavelength / nm
(d)
WE-1-20S-H
WE-1-60S-H
WE-1-60S
WE-1-40S
WE-1-20S
WE-1
IPCE / %
Wavelength / nm

Fig. 6

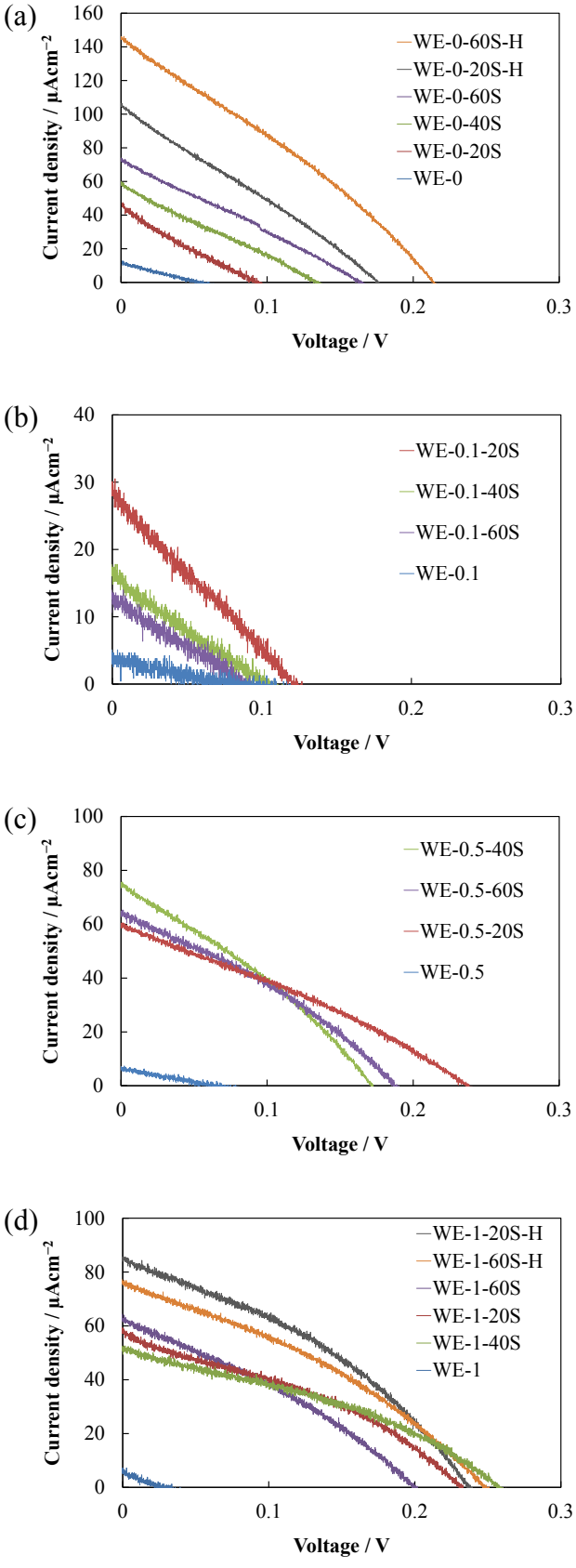
(a)
Current density / μAcm⁻²
Voltage / V
WE-0-60S-H
WE-0-20S-H
WE-0-60S
WE-0-40S
WE-0-20S
WE-0
(b)
Current density / μAcm⁻²
Voltage / V
WE-0.1-20S
WE-0.1-40S
WE-0.1-60S
WE-0.1
(c)
Current density / μAcm⁻²
Voltage / V
WE-0.5-40S
WE-0.5-60S
WE-0.5-20S
WE-0.5
(d)
Current density / μAcm⁻²
Voltage / V
WE-1-20S-H
WE-1-60S-H
WE-1-60S
WE-1-20S
WE-1-40S
WE-1

Fig. 7

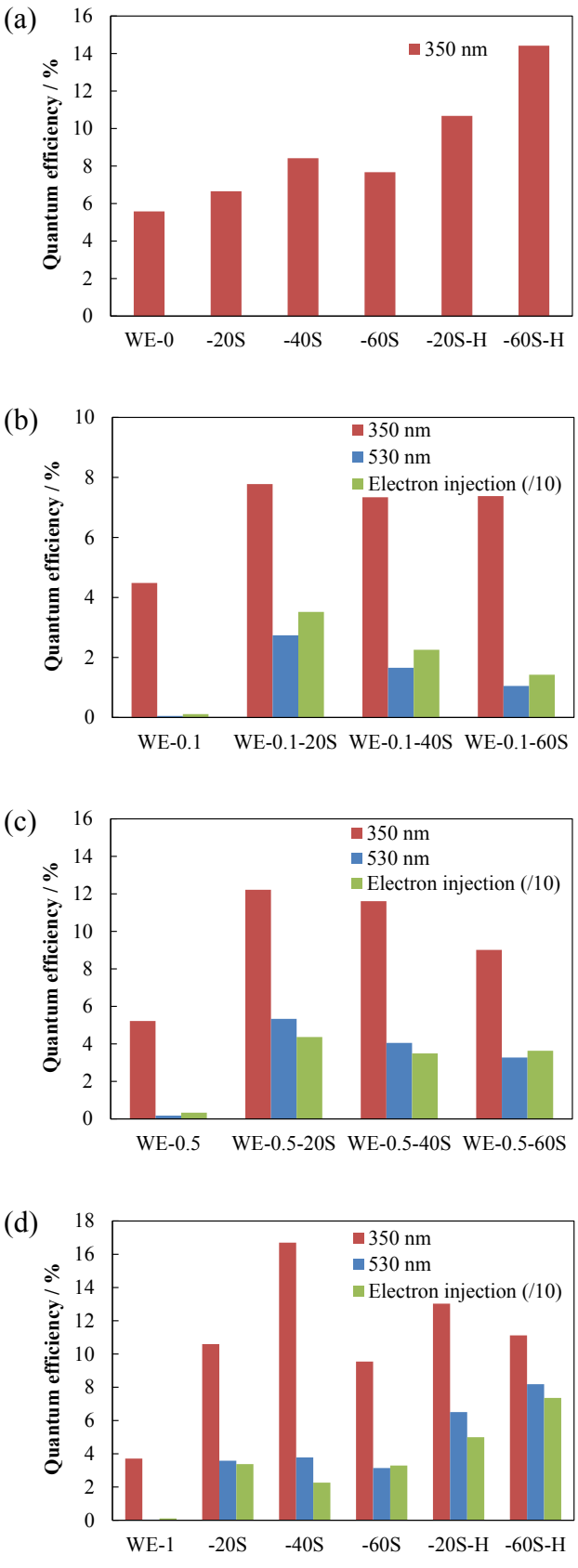
(a)
Quantum efficiency / %
350 nm
WE-0
-20S
-40S
-60S
-20S-H
-60S-H
(b)
Quantum efficiency / %
350 nm
530 nm
Electron injection (/10)
WE-0.1
WE-0.1-20S
WE-0.1-40S
WE-0.1-60S
(c)
Quantum efficiency / %
350 nm
530 nm
Electron injection (/10)
WE-0.5
WE-0.5-20S
WE-0.5-40S
WE-0.5-60S
(d)
Quantum efficiency / %
350 nm
530 nm
Electron injection (/10)
WE-1
-20S
-40S
-60S
-20S-H
-60S-H

Fig. 8

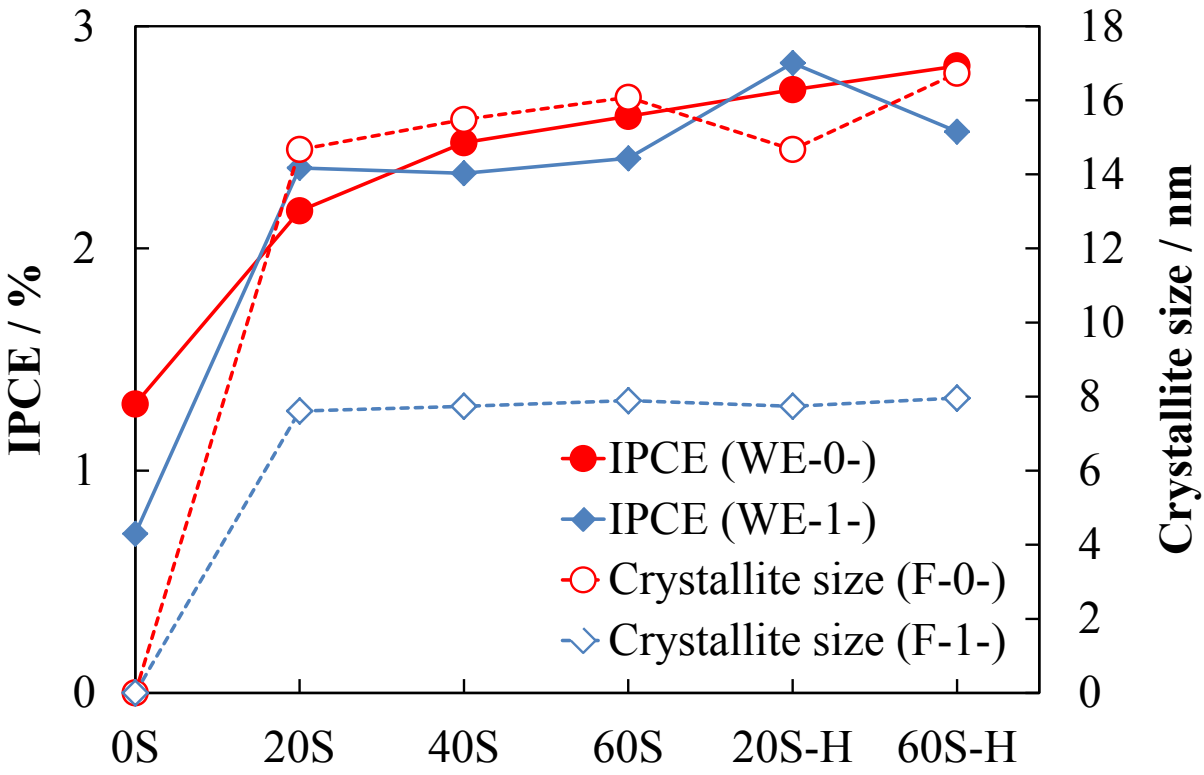
IPCE / %
Crystallite size / nm
3
2
1
0
18
16
14
12
10
8
6
4
2
0
0S
20S
40S
60S
20S-H
60S-H
IPCE (WE-0-)
IPCE (WE-1-)
Crystallite size (F-0-)
Crystallite size (F-1-)

Fig. 9

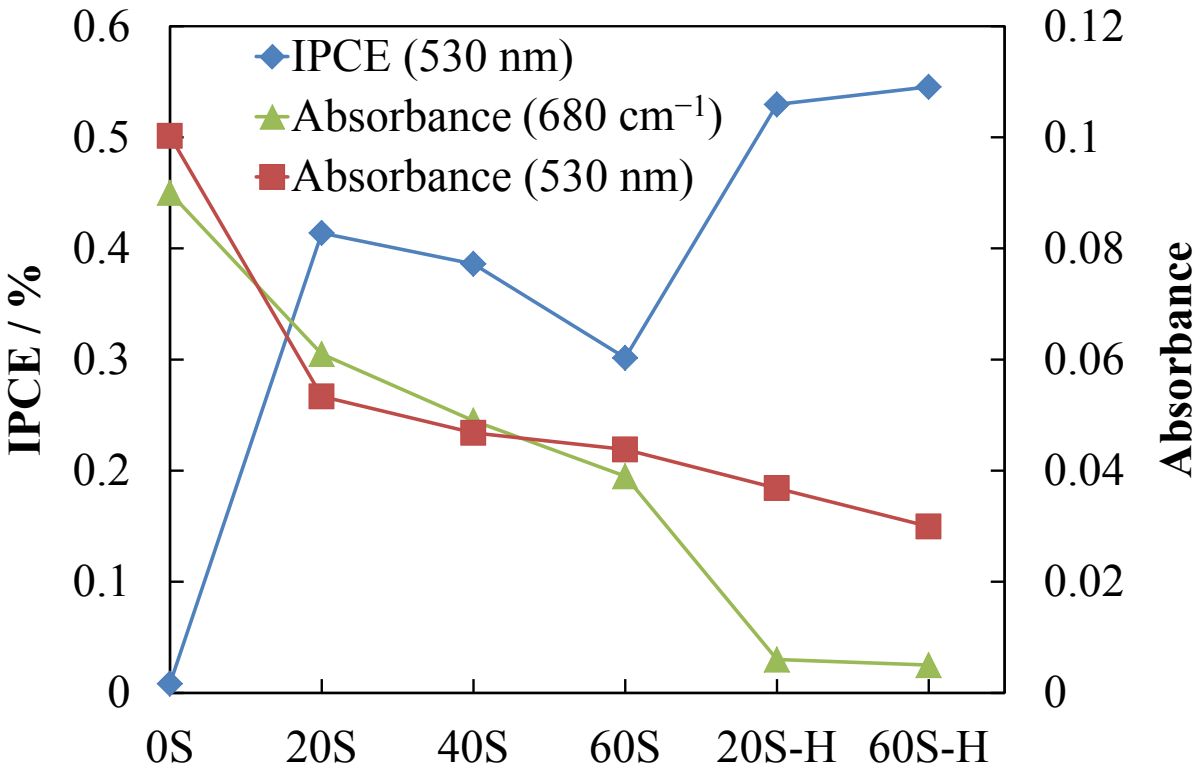
IPCE (530 nm)
Absorbance (680 cm⁻¹)
Absorbance (530 nm)
IPCE / %
Absorbance
0.6
0.5
0.4
0.3
0.2
0.1
0
0.12
0.1
0.08
0.06
0.04
0.02
0
0S
20S
40S
60S
20S-H
60S-H

Supporting Information

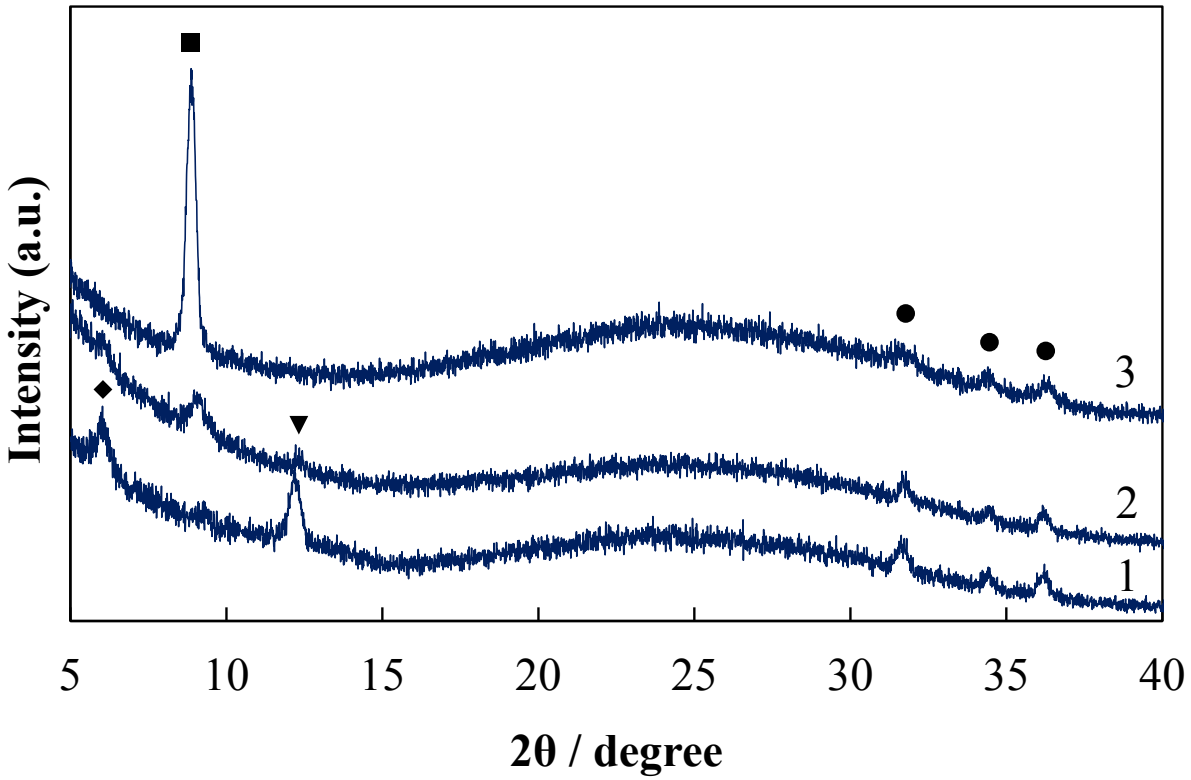

Fig. S1 XRD patterns of the films prepared from SG-*n*, which were steam treated for 40 min; (1) *n* = 0, F-0-40S, (2) *n* = 0.5, F-0.5-40S, and (3) *n* = 1, F-1-40S. The peaks are assigned to ZnO (●), $Zn_5(OH)_8(CH_3CO_2)_2 \cdot 2H_2O$ (♦), $Zn(CH_3CO_2)_2 \cdot 2H_2O$ (▼), and zinc hydroxide containing eosin Y(■)

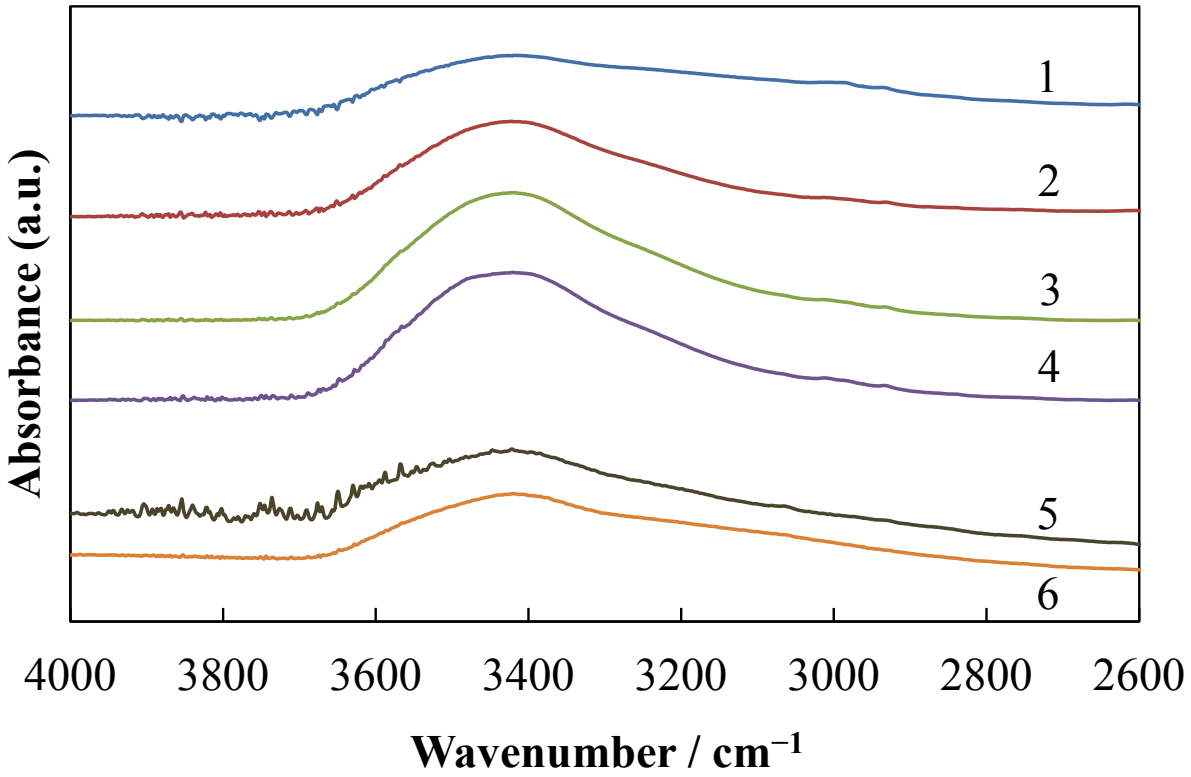

Fig. S2 FTIR spectra (4000–2600 cm^{-1}) of the films prepared from SG-1, (1) F-1, (2) F-1-20S, (3) F-1-40S, (4) F-1-60S, (5) F-1-20S-H, and (6) F-1-60S-H

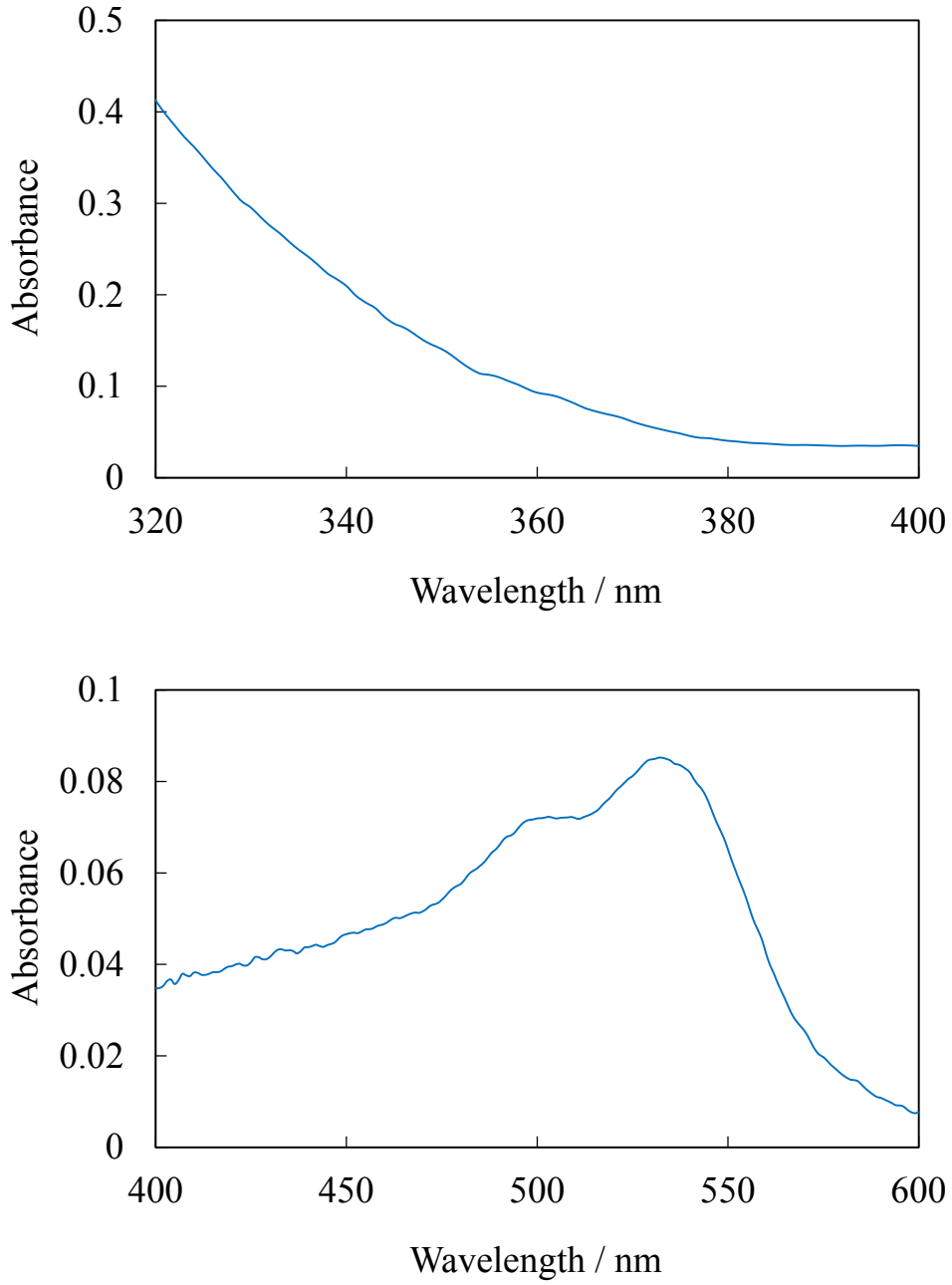

Fig. S3 UV–Vis absorption spectra of the electrode prepared from SG-0 which was steam-treated for 60-min, WE-0-60S, and then eosin Y- adsorbed.

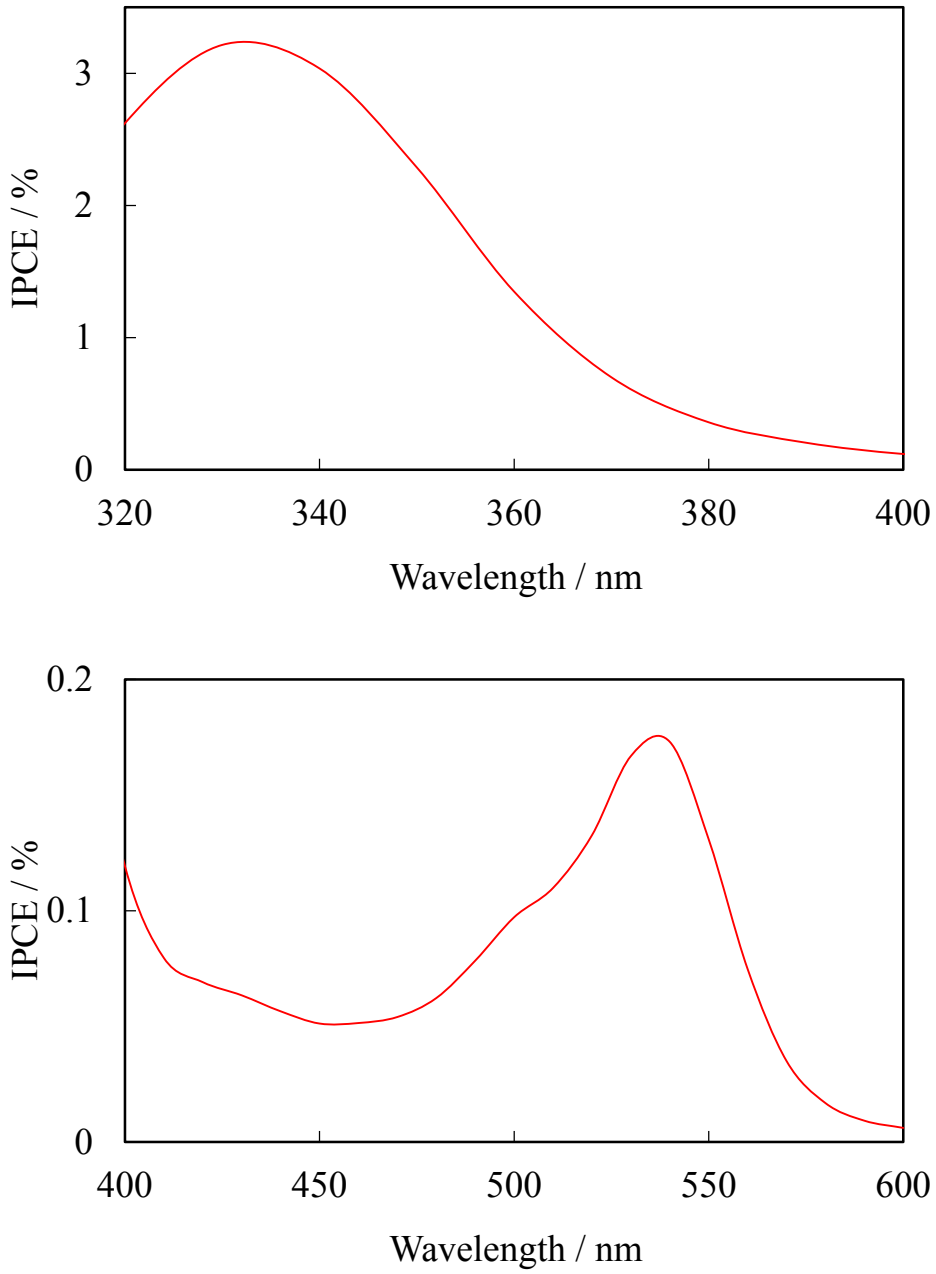

Fig. S4 IPCE spectra of the electrode prepared from SG-0 which was steam-treated for 60-min, WE-0-60S, and then eosin Y- adsorbed.